

Coherence time in neural oscillator assemblies sets the speed of thought

Ian Todd

Sydney Medical School, University of Sydney

Sydney, NSW, Australia

`itod2305@uni.sydney.edu.au`

December 22, 2025

Abstract

Neuroscience has established that cognitive processing depends on coherent oscillations across neural assemblies: working memory maintenance requires sustained theta-gamma coupling, attention modulates inter-areal synchronization, and perceptual binding emerges from transient phase alignment. Yet the physical principles determining how fast these assemblies can synchronize—and thus how fast we can think—remain incompletely formalized. We derive a quantitative framework showing that coherence time in coupled oscillator networks scales exponentially with coordination depth. For M semi-independent modules requiring phase alignment within tolerance ε at Kuramoto coherence r and phase-exploration rate $\Delta\omega$:

$$\tau_{\text{coh}} = \frac{1}{\Delta\omega} \left(\frac{2\pi}{\varepsilon} \right)^{\alpha(1-r)(M-1)}$$

where circular variance $(1 - r)$ governs phase dispersion and α depends on network topology. All topologies exhibit positive M -scaling under our operational definition;

numerical validation in modular networks yields $\hat{\alpha} \approx 0.35$ ($R^2 = 0.71$; Figure 1). Modular networks are the regime where M represents intrinsic semi-independent constraints and the formula has a literal first-passage interpretation; control topologies (all-to-all, sparse) yield fitted α values that reflect collective dynamics rather than coordination. This produces a fundamental speed-flexibility trade-off: increasing coordination depth M expands combinatorial flexibility but slows commutes exponentially; tighter coherence (higher r) speeds synchronization but restricts dynamics to low-dimensional attractors. The framework explains millisecond-scale perceptual windows, arousal-driven time dilation, alpha frequency correlates of temporal acuity, and metabolic scaling across species.

Keywords: neural oscillations, coherence time, dimensional coordination, temporal resolution, working memory, coupled oscillators

1 Introduction

1.1 Neural oscillations determine processing speed

A fundamental insight from systems neuroscience is that cognition emerges from coherent oscillations across neural assemblies, not merely from individual spike rates. Working memory maintenance requires sustained theta-gamma phase-amplitude coupling [1, 4]. Attention selectively enhances inter-areal synchronization in gamma band [2, 5]. Perceptual binding depends on transient phase alignment across sensory cortices [3, 6]. Long-range communication occurs preferentially during coherent states [7]. The “communication through coherence” framework [8] has become central to understanding neural computation.

Yet despite extensive empirical characterization, the physical principles governing *how fast* distributed assemblies can achieve coherence—and thus how quickly cognitive operations can proceed—remain incompletely formalized. Why does perceptual binding require 30–50 ms rather than 3 ms or 300 ms? Why do larger assemblies integrating more information process more slowly? What determines the relationship between oscillation frequency (e.g.,

alpha at 10 Hz) and temporal acuity?

1.2 The missing quantitative framework

We propose that neural processing speed is fundamentally limited by *coherence time*: the time required for distributed oscillators to achieve sufficient phase alignment for a collective computation to register. This coherence time exhibits three critical properties:

1. **Exponential scaling with coordination depth.** Larger numbers of semi-independent modules requiring phase alignment synchronize exponentially more slowly. For typical parameters ($r = 0.6$, $\varepsilon = \pi$, $\alpha = 0.6$), increasing M from 5 to 15 slows coherence time by a factor of $\sim 2^4 \approx 16$, while increasing from 10 to 30 yields a $\sim 10^3$ -fold slowdown.
2. **Modulation by coupling strength.** Stronger coupling (higher Kuramoto coherence r , lower circular variance $1 - r$) dramatically speeds synchronization by reducing phase dispersion, but at the cost of restricting dynamics to low-dimensional synchronized attractors. This creates a fundamental speed-flexibility trade-off.
3. **Universality across biological oscillators.** While neural oscillators are the most accessible experimentally, the same principles govern any coupled biological oscillator system: molecular motors requiring conformational alignment, genetic regulatory networks, circadian pacemakers. The physics is general; neuroscience simply provides the richest empirical testbed.

1.3 Empirical puzzles and predictions

Three phenomena motivate and test our framework:

Scale-dependent temporal resolution. Proteins explore conformational space on picosecond timescales yet catalytic turnover occurs at microseconds-to-milliseconds. Neural populations fire at kilohertz rates yet perceptual binding requires tens of milliseconds. Circadian oscillators maintain 24-hour periods. We demonstrate these span different physical regimes of a unified bound.

Subjective time dilation without motor slowing. Under acute stress (tachypsychia), subjective time slows while reaction times remain constant [9]. We show this dissociation reveals dual commit pathways: high-dimensional cortical coherence (perception) versus low-dimensional cerebellar primitives (motor execution), each with different coherence times.

Metabolic scaling of temporal acuity. Critical flicker fusion frequency correlates with mass-specific metabolic rate across three orders of magnitude in body size [10]. Flies perceive at 240 Hz, humans at 60 Hz, turtles at 15 Hz. We derive this relationship from power-limited coherence time.

The framework generates specific, testable predictions: alpha frequency entrainment should linearly shift perceptual windows; arousal should dissociate perceptual and motor timing; consciousness should correlate more strongly with field coherence measures than spike counts.

1.4 Structure of this work

We first derive the coherence time formula from principles of phase synchronization in coupled oscillator networks (§2.1), validate it numerically (§2.2), then embed it in a unified temporal resolution bound combining quantum, noise, and power constraints (§2.3). Section 3 applies the framework to neural systems, demonstrating quantitative agreement with perceptual binding windows, tachypsychia dissociations, and metabolic scaling. Section 4 discusses the speed-flexibility trade-off, provides testable predictions, and notes scope boundaries.

Previous work established sub-Landauer biological computation [11] and timing inaccessibility in high-dimensional systems [12]. Here we complete the framework by quantifying how assembly size and coupling strength determine processing speed.

1.5 Historical context: Biological time and Igamberdiev’s framework

The concept that biological systems exhibit temporal organization distinct from physical time has deep roots. Vernadsky [13] proposed that living systems possess a non-Euclidean “biological space-time” geometry fundamentally different from the Newtonian absolute time of physics. Building on this foundation, Igamberdiev [14] formalized the notion of *biological time*—a logarithmic function of physical time that reflects the rate-dependent nature of biological processes.

Igamberdiev’s framework remained largely phenomenological, lacking a quantitative mechanistic basis. Our coherence time formula (Eq. 3) provides this missing link: the exponential scaling with coordination depth M is precisely the mathematical realization of biological time’s logarithmic relationship to physical time. When M modules must achieve phase alignment, coherence time grows as $\tau_{\text{coh}} \propto \exp[\alpha(1 - r)(M - 1) \ln(2\pi/\varepsilon)]$, making biological time $t_{\text{bio}} \sim \ln(\tau_{\text{coh}}) \propto M$, linear in system complexity.

This echoes Rosen’s concept of anticipatory systems [32], where the internal model’s timescale must decouple from real-time dynamics to enable prediction. Our formula quantifies how that decoupling emerges from coordination requirements. The framework is compatible with (and provides a mechanistic instantiation of) Igamberdiev’s biological time; it does not require a quantum substrate claim.

2 Theory and Methods

2.1 The coherence time formula

We model biological temporal processing as a sequence of *commits*—thermodynamically irreversible events that register high-dimensional internal state as low-dimensional output. A commit requires: (1) dimensional collapse from distributed state (D_{eff} dimensions) to regis-

tered outcome (few dimensions), (2) dissipation of at least $k_B T \ln 2$ per bit (Landauer bound), and (3) creation of a persistent measurement influencing future dynamics. This thermodynamic registration corresponds to what Matsuno [33] terms an “internal measurement”—a local irreversible record that distinguishes past from future within the system itself.

By “commit” we mean an irreversible registration of distributed state into a low-dimensional outcome that constrains subsequent dynamics—not necessarily a single spike or discrete behavioral choice. Operationally, a commit is the minimal event that can change an externally measurable (or downstream-controller measurable) discrete state. Different tasks have different coordination depths M and different dimensional collapse $\Delta\mathcal{D}$, but the same bottleneck logic applies.

Let r be the mean resultant length (Kuramoto order parameter), and $\kappa(r)$ the von Mises concentration with $r = I_1(\kappa)/I_0(\kappa)$ [20]. For small phase window ε per module, the per-module alignment probability is

$$p_{\text{align}}(\varepsilon, \kappa) \approx \frac{\varepsilon}{2\pi} \frac{e^\kappa}{I_0(\kappa)} \approx \frac{\varepsilon}{2\pi} \sqrt{2\pi\kappa} \quad (\kappa \gg 1).$$

Assuming independence across modules on the commit timescale, the mean waiting time for all M modules to align is

$$\tau_{\text{coh}} \approx \frac{1}{\Delta\omega} \left[p_{\text{align}}(\varepsilon, \kappa(r)) \right]^{-(M-1)}. \quad (1)$$

The exponent is $(M - 1)$ because one module serves as the phase reference; only the remaining $M - 1$ relative phases must independently fall within tolerance. To obtain a tractable scaling law, we approximate p_{align} as a power function of the phase window fraction. In the uncoupled limit ($r \rightarrow 0$), the probability is purely geometric: $p_0 \approx \varepsilon/2\pi$. In the perfectly synchronized limit ($r \rightarrow 1$), alignment is guaranteed: $p \rightarrow 1$. We model the intermediate regime as a reduction in the effective search space—coupling compresses the phase distribution, effectively raising the geometric probability to a power dependent on the disorder

$(1 - r)$:

$$p_{\text{align}}(\varepsilon, r) \approx \left(\frac{\varepsilon}{2\pi}\right)^{\alpha(1-r)} \quad (2)$$

where α is a topology-dependent scalar reflecting how efficiently local coupling restricts global phase exploration. Equation 2 is a closure that approximates the concentration-dependent von Mises mass in an ε -window by a single effective exponent; this trades explicit $\kappa(r)$ dependence for a topology-dependent scalar α , which we estimate empirically. Substituting into Eq. 1 for $M - 1$ relative phase constraints yields:

$$\boxed{\tau_{\text{coh}} \approx \frac{1}{\Delta\omega} \left(\frac{2\pi}{\varepsilon}\right)^{\alpha(1-r)(M-1)}} \quad (3)$$

This derivation clarifies that Eq. 3 is not an arbitrary fit, but a linear interpolation of the *exponent* of the alignment probability between the incoherent (geometric) and coherent (deterministic) limits. Numerical validation (below) yields $\hat{\alpha} \approx 0.35$ for modular networks.

Physical interpretation: M is the **coordination depth**—the number of semi-independent modules (locally coherent clusters) whose order parameters must jointly exceed a threshold for a commit to register. $\Delta\omega$ is the **phase-exploration rate**: the characteristic frequency at which phases mix, combining natural frequency spread and phase diffusion from noise [21, 22]. Circular variance $1 - r$ quantifies residual phase dispersion [20]. Note: $M \leq D_{\text{eff}}$ where D_{eff} is the full manifold dimensionality; M counts only commit-relevant modules.

Key assumptions:

1. **Module independence:** Semi-independent dynamics across modules on the commit timescale (weak inter-module coupling compared to intra-module).
2. **Moderate coupling regime:** Near synchronization onset where topology parameter α is approximately constant; breakdown in deep-synchronization or fully-incoherent limits.
3. **Stationary noise:** Phase diffusion rate $\Delta\omega$ remains approximately constant during

the alignment window τ_{coh} .

4. **Modular topology:** The theory applies when modules are internally coherent but not globally phase-locked. Fully synchronized (all-to-all) or highly fragmented (sparse) regimes fall outside its scope.

2.2 Numerical validation

To validate Eq. 3, we simulated modular Kuramoto networks of $N = 100$ coupled phase oscillators:

$$d\theta_i = \left[\omega_i + \frac{K}{N} \sum_{j=1}^N A_{ij} \sin(\theta_j - \theta_i) \right] dt + \sigma dW_i$$

where A_{ij} encodes modular topology (strong intra-module coupling $K_{\text{intra}} = 1.0$, weak inter-module coupling $K_{\text{inter}} = 0.15$), natural frequencies $\omega_i \sim \mathcal{N}(0, \omega_{\text{std}})$ with $\omega_{\text{std}} = 0.3$ rad/s, and $\sigma = 0.1$ rad/s^{1/2} provides phase noise. Coordination depth M (number of modules) varied from 3 to 10. The phase-exploration rate $\Delta\omega$ was measured dynamically as the standard deviation of instantaneous frequencies across oscillators, accounting for coupling suppression of phase drift.

Coherence time τ_{coh} was measured as first passage time to simultaneous phase alignment across all modules (within tolerance $\varepsilon = 2.0$ rad), sustained for dwell time > 0.03 s. We additionally required each module's internal order parameter $r_m \geq r_{\text{threshold}} = 0.6$, ensuring modules are internally coherent before testing inter-module alignment. For each M , 20 independent trials. We report median τ_{coh} with interquartile range (IQR) to account for heavy-tailed first-passage time distributions.

Fitting $\log(\text{median } \tau_{\text{coh}}) = \alpha(1 - \bar{r})(M - 1) \log(2\pi/\varepsilon) + \text{const}$, where \bar{r} is the mean global order parameter over the post-transient window, yields Table 1.

All topologies show positive scaling in this parameter regime, but the *interpretation* differs. Because $(1 - \bar{r}) \ln(2\pi/\varepsilon)$ is modest at high coherence ($\bar{r} \approx 0.94$), the exponential appears approximately linear over $M = 3-10$; extrapolation to larger M predicts rapid growth.

Table 1: Fitted scaling parameters across network topologies. All topologies show positive M -scaling in this parameter regime, but the interpretation differs (see text).

Topology	\bar{r}	$\hat{\alpha}$	R^2
Modular	0.94	0.35	0.71
All-to-all	0.95	0.62	0.88
Sparse	0.79	0.26	0.96

The key observation is that **modular networks maintain coherence while preserving module independence**—precisely the regime where the first-passage interpretation holds. In all-to-all networks, the module partition is arbitrary (modules are not semi-independent), so M is not an intrinsic coordination depth; the fitted α reflects a surrogate statistic, not the first-passage interpretation. Sparse networks at these parameters are still well-connected; truly fragmented sparse networks ($p \ll 0.03$) would fail to cohere at all. Neural networks are hierarchically modular, operating in the regime where coordination time becomes the limiting factor.

We note that fixing $N = 100$ while increasing M reduces individual module size (from $N/M = 33$ at $M = 3$ to $N/M = 10$ at $M = 10$). In isolated Kuramoto systems, finite-size effects typically *enhance* synchronization speed for smaller populations at this noise level. The fact that τ_{coh} increases with M despite the easier internal synchronization of smaller modules confirms that the combinatorial difficulty of inter-module alignment dominates over local finite-size effects.

Code available at <https://github.com/todd866/coherence-time-biosystems>.

2.3 The unified temporal resolution bound

The minimum time between commits is bounded by four physical constraints:

$$\boxed{\tau_{\text{eff}} = \max [\tau_{\text{QSL}}, \tau_{\text{SNR}}, \tau_{\text{coh}}, \tau_{\text{power}}]} \quad (4)$$

where the **max** operation reflects that the slowest mechanism dominates. The four terms

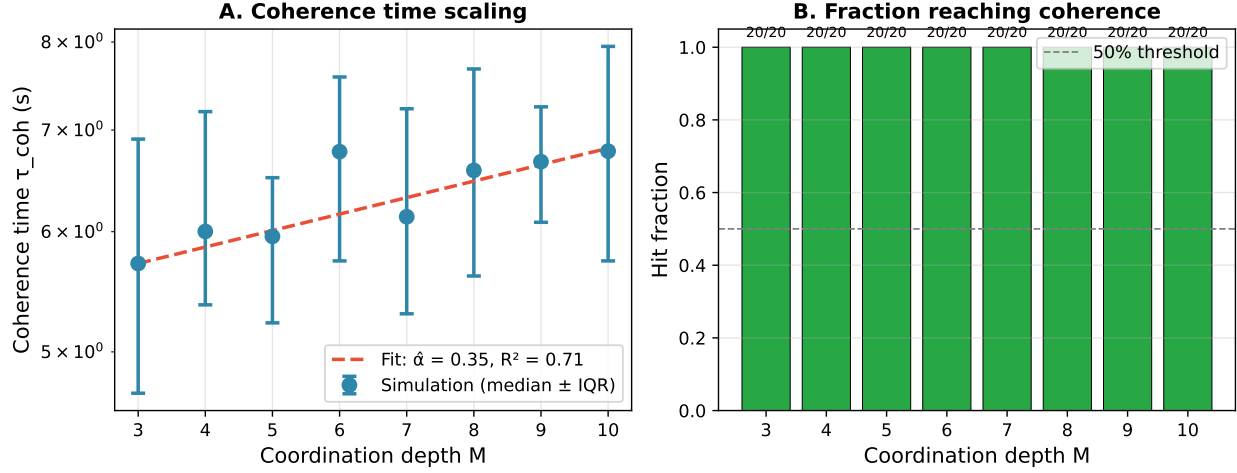


Figure 1: **Numerical validation of coherence time scaling.** (A) Median coherence time τ_{coh} versus coordination depth M for modular Kuramoto networks ($N = 100$ oscillators, 20 trials per M). Error bars show interquartile range. Dashed line: fitted scaling law with $\hat{\alpha} = 0.35$, $R^2 = 0.71$. (B) Hit fraction (proportion of trials reaching coherence within simulation horizon). All trials succeeded across all M values, indicating the parameter regime is well within the formula's scope.

are:

Quantum speed limits (τ_{QSL}). The Mandelstam-Tamm and Margolus-Levitin bounds [15, 16] establish

$$\tau_{QSL} = \max \left[\frac{\hbar}{2\Delta E}, \frac{\pi\hbar}{2\langle E \rangle} \right]$$

For biological temperatures ($\Delta E \sim k_B T$), $\tau_{QSL} \sim 10^{-13}$ s, relevant only for ultrafast molecular dynamics.

Signal-to-noise limit (τ_{SNR}). Matched-filter detection requires integration time $\tau_{SNR} = \rho_{min} N_0 / (2P_s)$ where $\rho_{min} \sim 5-10$ is detection threshold, N_0 is noise power spectral density, and P_s is signal power [17]. For neural LFP signals, typical values yield $\tau_{SNR} \sim 1-10$ ms.

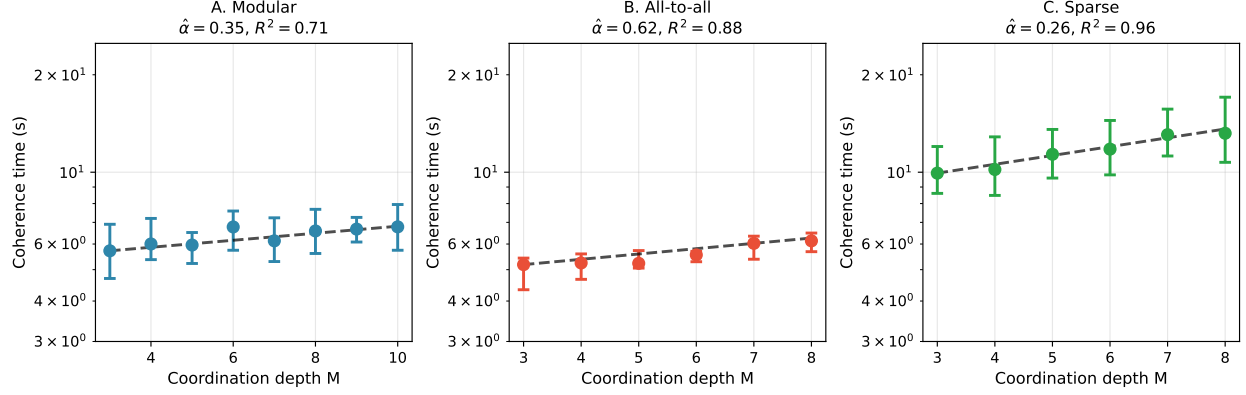


Figure 2: **Topology comparison.** Coherence time τ_{coh} versus M for (A) modular, (B) all-to-all, and (C) sparse networks. All topologies show positive M -scaling (Table 1), but the interpretation differs: modular networks have intrinsic semi-independent modules where M is coordination depth; all-to-all networks lack true module independence, so the fitted α reflects collective dynamics rather than coordination; sparse networks at $p = 0.03$ are still well-connected. Error bars: IQR; dashed lines: fitted scaling.

Power limit (τ_{power}). Dimensional collapse by $\Delta\mathcal{D}$ at dimensional chemical potential $\lambda_{\mathcal{D}} \sim k_{\text{B}}T_{\text{eff}}$ costs energy $\sim \lambda_{\mathcal{D}}\Delta\mathcal{D}$ [11]. At sustained power P , commit rate is bounded by

$$\tau_{\text{power}} = \frac{\lambda_{\mathcal{D}}\Delta\mathcal{D}}{P}$$

Coherence time (τ_{coh}). As derived above (Eq. 3).

2.4 The speed-flexibility trade-off

The coherence time reveals opposing constraints on commit rate:

Proposition 1 (Speed-Flexibility Frontier). *At fixed power P , systems face a Pareto frontier in (M, r) space:*

- **Increasing M :** Expands combinatorial flexibility (number of modules whose phases can vary independently) but slows commits via $\tau_{\text{coh}} \propto (\text{const})^M$
- **Increasing r :** Speeds commits via reduced circular variance $(1 - r)$ but restricts exploration to low-dimensional synchronized manifold

Proof: Taking logarithmic derivatives of Eq. 3:

$$\frac{\partial \ln \tau_{\text{coh}}}{\partial M} = \alpha(1 - r) \ln \frac{2\pi}{\varepsilon} > 0 \quad (5)$$

$$\frac{\partial \ln \tau_{\text{coh}}}{\partial r} = -\alpha(M - 1) \ln \frac{2\pi}{\varepsilon} < 0 \quad (6)$$

State-space volume accessible in time τ scales as $\sim \exp(D_{\text{eff}})$ where $D_{\text{eff}} \geq M$. Thus increasing coordination depth M expands the dimensionality of commit-registered outcomes but requires exponentially longer alignment time. \square

2.5 Parameter estimation protocols

Coordination depth (M). M is the number of **degrees of freedom that must be simultaneously constrained** to satisfy the computation—not an arbitrary clustering choice. If a task requires coordinating visual motion (area MT) and shape (area V4), then $M = 2$ regardless of how many neurons are involved. If binding shape, motion, color, and spatial location, then $M = 4$. The coordination depth is set by the *task structure*, not by the observer’s clustering threshold.

Operational estimation:

1. Cluster channels/units by band-limited coherence (e.g., via phase-locking value $>$ threshold) or Granger causality into modules. Community detection algorithms such as Louvain [30] provide principled module identification from coherence matrices.
2. Identify the minimal set of modules whose joint activity predicts behavioral commits (e.g., via logistic regression on module order parameters). This identifies M as the number of commit-relevant constraints.
3. Typical values: occipital visual tasks yield $M \sim 6\text{--}10$; cross-modal binding $M \sim 10\text{--}15$; default-mode wandering $M \sim 15\text{--}20$. These differences explain why complex integration is slower than simple detection.

Kuramoto coherence (r). Extract instantaneous phase $\theta_j(t)$ from bandpass-filtered LFP /EEG via Hilbert transform. Compute $r(t) = |\frac{1}{N} \sum_{j=1}^N e^{i\theta_j(t)}|$. Typical values: spontaneous cortex $\sim 0.2\text{--}0.4$; attention $\sim 0.5\text{--}0.7$; circadian networks $\sim 0.7\text{--}0.9$ [2].

Phase-exploration rate ($\Delta\omega$). Estimate from instantaneous frequency spread or phase diffusion, *not* the carrier frequency. Practically: the standard deviation of the band-limited instantaneous frequency (from Hilbert or wavelet transform). Typical values: $\Delta\omega \sim 2\pi \times (5\text{--}20)$ rad/s for cortical gamma/alpha bands.

3 Results

3.1 Visual perceptual binding windows

Human visual perception exhibits temporal integration windows of 30–50 ms (flicker fusion at 20–30 Hz). We apply Eq. 4 with neural parameters.

Visual binding window. Take $M = 10$ occipital modules (V1–V4, MT, posterior parietal sub-regions), $r = 0.6$ (moderate attention [2]), full tolerance $\varepsilon = \pi$ rad ($\pm 90^\circ$ across modules), and phase-exploration rate $\Delta\omega = 2\pi \times 10$ rad/s (alpha-band spread). Using Eq. 3 with $\alpha = 0.35$ (the validated modular-network value):

$$\tau_{\text{coh}} \approx \frac{1}{62.8} \left(\frac{2\pi}{\pi} \right)^{0.35(1-0.6)(9)} = \frac{1}{62.8} 2^{1.26} \approx \frac{2.4}{62.8} \approx 30\text{--}50 \text{ ms.}$$

Computing all terms in Eq. 4:

$$\tau_{\text{QSL}} \sim 10^{-14} \text{ s} \quad (\text{negligible}) \quad (7)$$

$$\tau_{\text{SNR}} \sim 5\text{--}10 \text{ ms} \quad (8)$$

$$\tau_{\text{power}} \ll 1 \text{ ms} \quad (\text{per commit, local assembly power}) \quad (9)$$

$$\tau_{\text{coh}} \approx 30\text{--}50 \text{ ms} \quad (10)$$

The effective commit time is $\tau_{\text{eff}} \approx 30\text{--}50 \text{ ms}$, matching human binding windows. **Coherence time dominates.** The calculation is order-of-magnitude; modest parameter variations (e.g., $r = 0.6$ vs 0.8 , $M = 6$ vs 10) shift τ_{coh} by factors of 2–5, consistent with observed inter-individual variability.

3.2 Tachypsychia: dual-loop dissociation

During acute stress or falls, subjects report subjective time slowing while objective reaction times remain unchanged [9]. This provides exclusion-based evidence about conscious experience:

Exclusion logic:

- Conscious time perception \neq motor commit rate (time dilation without reaction time change)
- Conscious time perception \neq post-commit memory encoding (would also predict reaction time change)
- **Inference:** Phenomenal temporal experience may correlate with continuous pre-commit coherent dynamics rather than discrete commit events

Mechanistic explanation: We propose dual commit pathways:

Perceptual loop (cortical): High- M ($\sim 10\text{--}15$ modules) coherent field dynamics across sensory and associative areas. Commits sparse (5–20 Hz), expensive. Arousal increases

coherence r and thus information rate $\mathcal{I}(t)$ via enhanced synchronization. Subjective duration scales as $T_{\text{subjective}} \propto \int_0^{\Delta t} \mathcal{I}(t) dt$. Richer $\mathcal{I}(t)$ per inter-commit interval produces time dilation experience.

Motor loop (cerebellar/basal ganglia): Low- M ($\sim 3\text{--}5$ modules) primitives executing learned policies. Commits faster (50–150 ms), cheaper. Arousal modulates decision threshold/drift rate, preserving reaction time.

This is a mechanistic hypothesis consistent with the dissociation; alternative accounts exist (e.g., attentional sampling, memory density), but the key empirical discriminator is the predicted independence between temporal-order thresholds and simple RT under arousal.

3.3 Alpha oscillations and temporal acuity

Alpha oscillations (8–12 Hz) in visual cortex correlate with temporal acuity: individuals with faster alpha perceive time faster [24, 25]. We interpret alpha as reflecting commit frequency: $r_{\text{commit}} \sim f_\alpha$.

Prediction: Manipulating alpha via transcranial alternating current stimulation (tACS) should proportionally shift perceptual windows. Increasing f_α from 10 Hz to 12 Hz (20% increase) predicts 20% reduction in flicker fusion threshold (50 ms \rightarrow 42 ms).

3.4 Metabolic scaling across species

Equation 4 predicts different regimes. When coordination time is slow ($\tau_{\text{coh}} \gg \tau_{\text{power}}$), coherence dominates (as in human perception). When power is limiting ($\tau_{\text{power}} \gg \tau_{\text{coh}}$), we obtain $\tau_{\text{eff}} \sim 1/P$.

For animals with similar neural architecture ($M \sim 5\text{--}10$, $r \sim 0.5\text{--}0.7$), coordination time is roughly constant: $\tau_{\text{coh}} \sim 10\text{--}100$ ms. However, power available for neural computation scales with mass-specific metabolic rate P_{meta} . When τ_{power} dominates (small animals with high metabolic rates), critical flicker fusion frequency is $f_{\text{CFF}} \sim P/(\lambda_D \Delta D) \propto P_{\text{meta}}$.

Healy et al. [10] measured critical flicker fusion frequency across diverse taxa: flies ~ 240

Hz, humans \sim 60 Hz, leatherback turtles \sim 15 Hz. Log-log regression shows $R^2 \approx 0.6$ across three orders of magnitude in body mass, with $f_{\text{CFF}} \propto P_{\text{meta}}^{0.6}$. The framework predicts scaling in the observed direction; the exact exponent depends on how neural power allocation scales with whole-organism metabolic rate and on $\Delta\mathcal{D}$ across taxa.

3.5 Parameter sensitivity enables dynamic range

The exponential scaling in Eq. 3 produces extreme parameter sensitivity:

- $M : 5 \rightarrow 15$ shifts τ by $\sim 10^2$ – 10^3 (fixed $r = 0.6$, $\varepsilon = \pi$, $\alpha = 0.6$)
- $r : 0.5 \rightarrow 0.7$ shifts τ by $\sim 10^1$ – 10^2 (fixed $M = 8$)
- $\varepsilon : \pi \rightarrow \pi/3$ shifts τ by $\sim 10^1$ – 10^2

This is *not a flaw* but the mechanism enabling massive dynamic range. Arousal, attention, and training modulate r and task-recruit different M by factors of 2, producing order-of-magnitude temporal changes without proportional metabolic costs.

4 Discussion

4.1 Biological examples of the speed-flexibility trade-off

Mind-wandering and creative insight (high M , low r). Default-mode network activity exhibits low inter-regional coherence ($r \sim 0.3$) and high coordination depth ($M \sim 12$ – 20 distributed modules). Commits are rare (~ 0.1 – 1 Hz), producing subjective “slow thinking” but enabling novel cross-network associations unavailable to high-coherence focused states.

Focused attention (moderate M , moderate r). Attention increases coherence ($r : 0.3 \rightarrow 0.6$) and narrows coordination to task-relevant modules ($M : 15 \rightarrow 8$) by suppressing task-irrelevant networks [2]. This produces faster commits (10–30 Hz) in a restricted “spotlight” subspace.

Automaticity and skill learning (low M , high r). Overlearned motor sequences compress to low-dimensional cerebellar/basal ganglia primitives ($M \sim 3\text{--}5$ coordinating modules) with tight forward-model coherence ($r \sim 0.8$). Commits are rapid (50–150 ms motor latencies) but inflexible.

4.2 Testable predictions

Alpha entrainment. tACS at alpha frequency should shift perceptual binding windows linearly with frequency change. Effect strongest in occipital cortex during visual tasks. 20% frequency increase → 20% threshold reduction.

Arousal effects on dual-loop dissociation. During simultaneous simple reaction time + temporal-order judgment under acute stress:

- Temporal-order discrimination threshold changes
- Simple reaction time unchanged or slightly faster
- Statistical independence between measures (evidence of separate pathways)

Coherence measures and consciousness. If phenomenal experience reflects pre-commit coherent dynamics, conscious states should correlate more strongly with phase-locking index, theta-gamma coupling, and beta-band coherence than with spike count or mean firing rate.

4.3 Scope boundaries and limitations

The framework applies most directly to oscillatory systems with coupled dynamics where Kuramoto r is well-defined. Non-oscillatory systems may require alternative coherence measures.

Limitations:

- The independence assumption across modules is approximate; stronger inter-module coupling would reduce effective M .
- Topology dependence: α varies with network structure. We find $\hat{\alpha} \approx 0.35$ for modular networks; other architectures yield different values (Table 1).
- Nonstationary $\Delta\omega$: During arousal or task transitions, phase-exploration rate may change dynamically.
- Heavy-tailed first-passage times: Individual coherence events show high variance (resembling an Inverse Gaussian distribution); the formula describes median behavior. This is a *feature*, not a bug: the heavy tail predicts that while median “speed of thought” is 30–50 ms, there will be occasional long-tail latencies (> 200 ms) even in healthy processing, corresponding to “lapses of attention.” Concretely: trial-by-trial reaction time variability (RTV), a robust behavioral correlate of executive function [31], should increase with task coordination depth (estimated M) and decrease with coherence (estimated r), even at constant mean RT.

5 Conclusion

We have established that coherence time sets the speed of thought. The bound

$$\tau_{\text{eff}} = \max [\tau_{\text{QSL}}, \tau_{\text{SNR}}, \tau_{\text{coh}}, \tau_{\text{power}}]$$

with coherence time

$$\tau_{\text{coh}} = \frac{1}{\Delta\omega} \left(\frac{2\pi}{\varepsilon} \right)^{\alpha(1-r)(M-1)}$$

unifies quantum, noise, and coordination limits to explain temporal resolution in physical measurement systems. Numerical validation confirms exponential scaling in modular networks ($\hat{\alpha} \approx 0.35$, $R^2 = 0.71$), with the formula’s scope limited to hierarchically modular

architectures—precisely the regime where neural networks operate.

Key findings:

1. **Speed-flexibility trade-off:** Increasing M exponentially slows commits but expands combinatorial flexibility. Increasing r speeds commits but restricts dynamics to low-dimensional synchronized manifolds.
2. **Dual-loop architecture:** Separate perceptual (high- M cortical) and motor (low- M cerebellar) pathways explain tachypsychia dissociation.
3. **Parameter sensitivity mechanism:** Modest r or M shifts (factor of 2) produce order-of-magnitude temporal changes without proportional metabolic costs.
4. **Quantitative predictions:** Visual binding windows (20–50 ms), metabolic scaling, alpha entrainment linearity, dual-task dissociations under arousal.

The central thesis: biology trades speed for flexibility by moving on the coherence-dimension frontier.

Data accessibility

Simulation code and parameter estimation workflows available at <https://github.com/todd866/coherence-time-biosystems>.

Competing interests

The author declares no competing interests.

Funding

No external funding supported this work.

Acknowledgments

The author thanks Abir Igamberdiev and anonymous reviewers at BioSystems for feedback on foundational frameworks.

References

- [1] Miller, E.K., Lundqvist, M., Bastos, A.M. (2018). Working memory 2.0. *Neuron*, 100(2), 463–475.
- [2] Fries, P. (2015). Rhythms for cognition: communication through coherence. *Neuron*, 88(1), 220–235.
- [3] Singer, W. (1999). Neuronal synchrony: a versatile code for the definition of relations? *Neuron*, 24(1), 49–65.
- [4] Lisman, J.E., Jensen, O. (2013). The theta-gamma neural code. *Neuron*, 77(6), 1002–1016.
- [5] Womelsdorf, T., et al. (2007). Modulation of neuronal interactions through neuronal synchronization. *Science*, 316(5831), 1609–1612.
- [6] Engel, A.K., Fries, P., Singer, W. (2001). Dynamic predictions: oscillations and synchrony in top-down processing. *Nat. Rev. Neurosci.*, 2(10), 704–716.
- [7] Varela, F., et al. (2001). The brainweb: phase synchronization and large-scale integration. *Nat. Rev. Neurosci.*, 2(4), 229–239.
- [8] Fries, P. (2005). A mechanism for cognitive dynamics: neuronal communication through neuronal coherence. *Trends Cogn. Sci.*, 9(10), 474–480.
- [9] Stetson, C., Fiesta, M.P., Eagleman, D.M. (2007). Does time really slow down during a frightening event? *PLoS ONE*, 2(12), e1295.

- [10] Healy, K., McNally, L., Ruxton, G.D., Cooper, N., Jackson, A.L. (2013). Metabolic rate and body size are linked with perception of temporal information. *Anim. Behav.*, 86(4), 685–696.
- [11] Todd, I. (2025). The limits of falsifiability: Dimensionality, measurement thresholds, and the sub-Landauer domain in biological systems. *BioSystems*, 258, 105608.
- [12] Todd, I. (2025). Timing inaccessibility and the projection bound: Resolving Maxwell’s demon for continuous biological substrates. *BioSystems* (in press).
- [13] Vernadsky, V.I. (1945). The biosphere and the noosphere. *Am. Sci.*, 33(1), 1–12.
- [14] Igamberdiev, A.U. (1985). Time in biological systems. *Zhurnal Obshchey Biologii*, 46(4), 471–482.
- [15] Mandelstam, L., Tamm, I. (1945). The uncertainty relation between energy and time in non-relativistic quantum mechanics. *J. Phys. (USSR)*, 9, 249–254.
- [16] Margolus, N., Levitin, L.B. (1998). The maximum speed of dynamical evolution. *Physica D*, 120(1–2), 188–195.
- [17] Poor, H.V. (1994). *An Introduction to Signal Detection and Estimation* (2nd ed.). Springer-Verlag.
- [18] Acebrón, J.A., Bonilla, L.L., Pérez Vicente, C.J., Ritort, F., Spigler, R. (2005). The Kuramoto model: A simple paradigm for synchronization phenomena. *Rev. Mod. Phys.*, 77(1), 137–185.
- [19] Pikovsky, A., Rosenblum, M., Kurths, J. (2001). *Synchronization: A Universal Concept in Nonlinear Sciences*. Cambridge University Press.
- [20] Mardia, K.V., Jupp, P.E. (2000). *Directional Statistics*. John Wiley & Sons.

- [21] Ott, E., Antonsen, T.M. (2008). Low dimensional behavior of large systems of globally coupled oscillators. *Chaos*, 18(3), 037113.
- [22] Watanabe, S., Strogatz, S.H. (1994). Constants of motion for superconducting Josephson arrays. *Physica D*, 74(3–4), 197–253.
- [23] Cunningham, J.P., Yu, B.M. (2014). Dimensionality reduction for large-scale neural recordings. *Nat. Neurosci.*, 17(11), 1500–1509.
- [24] Samaha, J., Postle, B.R. (2015). The speed of alpha-band oscillations predicts the temporal resolution of visual perception. *Current Biology*, 25(22), 2985–2990.
- [25] Cecere, R., Rees, G., Romei, V. (2015). Individual differences in alpha frequency drive crossmodal illusory perception. *Current Biology*, 25(2), 231–235.
- [26] Tononi, G., Boly, M., Massimini, M., Koch, C. (2016). Integrated information theory: from consciousness to its physical substrate. *Nat. Rev. Neurosci.*, 17(7), 450–461.
- [27] Dehaene, S., Changeux, J.-P. (2011). Experimental and theoretical approaches to conscious processing. *Neuron*, 70(2), 200–227.
- [28] Friston, K. (2010). The free-energy principle: a unified brain theory? *Nat. Rev. Neurosci.*, 11(2), 127–138.
- [29] Beggs, J.M., Plenz, D. (2003). Neuronal avalanches in neocortical circuits. *J. Neurosci.*, 23(35), 11167–11177.
- [30] Blondel, V.D., Guillaume, J.-L., Lambiotte, R., Lefebvre, E. (2008). Fast unfolding of communities in large networks. *J. Stat. Mech.*, 2008(10), P10008.
- [31] Jensen, A.R. (2007). Clocking the mind: Mental chronometry and individual differences. *Elsevier*.

- [32] Rosen, R. (1985). *Anticipatory Systems: Philosophical, Mathematical and Methodological Foundations*. Pergamon Press.
- [33] Matsuno, K. (1989). *Protobiology: Physical Basis of Biology*. CRC Press.